International Journal of Multiphase Flow 34 (2008) 997–1007

Contents lists available at ScienceDirect

International Journal of Multiphase Flow

journal homepage: www.elsevier.com/locate/ijmulflow

Horizontal laminar flow of coarse nearly-neutrally buoyant particles in non-Newtonian conveying fluids: CFD and PEPT experiments compared

M. Eesa, M. Barigou *

School of Chemical Engineering, The University of Birmingham, Edgbaston, Birmingham B15 2TT, UK

ARTICLE INFO

Article history:
Received 20 December 2007
Received in revised form 7 May 2008
Accepted 17 June 2008
Available online 25 June 2008

Keywords:
CFD
Eulerian–Eulerian
Non-Newtonian fluid
PEPT
Pressure drop
Solid–liquid
Velocity profile

ABSTRACT

The horizontal flow of coarse particle suspensions in non-Newtonian carrier fluids was numerically simulated using an Eulerian–Eulerian CFD model. This study was concerned with nearly-neutrally buoyant particles of 5 and 10 mm diameter conveyed by fluids of Ellis rheology in laminar flow, in a 45 mm diameter pipe at concentrations up to 41% v/v. CFD predictions of solid phase velocity profiles and passage times were compared to experimental data obtained by a Positron Emission Particle Tracking (PEPT) technique and Hall effect sensors, and a very good agreement was obtained considering the complexity of the flows studied. CFD predictions of solid–liquid pressure drop were compared to a number of relevant correlations gleaned from the literature. Only one of them showed a good agreement over the whole range of conditions studied. Other correlations generally showed large deviations from CFD, and their limitations in predicting the influence of solids concentration and particle size have been demonstrated. Overall, it emerged that for the flows studied, CFD was capable of giving predictions of pressure drop which were probably better and more reliable than the correlations available in the literature.

1. Introduction

Solid–liquid flow is encountered in a wide variety of situations from hygienic movement and processing of food and pharmaceutical products, through chemicals, oil, mining and construction applications, to the secure transportation of effluent and waste products. Although most applications use water as the carrier medium, there are now many industrial plants, e.g. food, chemical, oil, mining, and power generation industries, where particles are transported in a variety of liquids which may be highly viscous and may exhibit non-Newtonian behaviour. The complexity of these solid–liquid flows is reflected in the number of independent variables generally involved which causes the flow behaviour of these systems to vary over a tremendous range (Abulnaga, 2002). The pipeline (diameter, length, roughness, fittings), the properties of the solids (size and size distribution, shape, density, strength) and of the liquid (density, rheology), and the operating conditions (mixture flowrate, solids concentration) all influence the nature of the flow and the pressure gradient.

Fine particles tend to form reasonably homogeneous suspensions and are usually treated as such. Concentrated suspensions of fine particles may exhibit Newtonian or non-Newtonian behaviour, and are frequently transported in laminar flow where they behave essentially as single phase pseudoplastic (i.e. shear-thinning) liquids, e.g. flocculated kaolin and coal suspensions. Existing models for describing them are based on the principles of continuum mechanics. Thus, pressure drop, for example, is estimated by single phase flow methods using an effective density and viscosity for the suspension (Chhabra and Richardson, 1999).

The vast majority of the documented data on solid–liquid flow relate to water-based slurries of fine particles. There is, therefore, a clear need for experimental data and models to describe the flow of coarse solid–liquid mixtures as they are relevant to a number of industrial applications including the conveying of particulate food mixtures, gravel, and coal lumps. In particular, there is a severe lack of information on the flow of such coarse solid–liquid suspensions in viscous Newtonian and non-Newtonian carrier media. The presence of large particles in a viscous Newtonian or non-Newtonian liquid gives rise to a heterogeneous mixture of complex rheology where the assumption of a continuum as used in fine suspension is clearly inapplicable. Inertial effects, gravitational forces, particle–particle and particle–wall interactions affect the flow of the solid phase giving rise to a different particle behaviour and flow patterns from the carrier fluid.

Viscous Newtonian/non-Newtonian carriers are used because: (a) they are in some cases dictated by the process, e.g. Newtonian heavy oil to transport solids out of wells, and continuous thermal processing of particulate food products in non-Newtonian fluids.

* Corresponding author. Tel.: +44 121 414 5277; fax: +44 121 414 5324.
E-mail address: m.barigou@bham.ac.uk (M. Barigou).

0301-9322/$ - see front matter © 2008 Elsevier Ltd. All rights reserved.
doi:10.1016/j.ijmultiphaseflow.2008.06.003

In the latter case, the process can be subjected to a wide distribution of particle concentrations, velocities, residence times, and temperatures, thereby causing a wide and largely unpredictable distribution of those quality changes that are induced in the food by the heat treatment. The liquid and solid phases sterilise at different times and, therefore, knowledge of the distribution of both liquid and particle velocities/residence times are essential for a sound process design; and (b) when the flow is laminar, the transport of coarse particles in fluids of non-Newtonian rheology offers certain advantages: (i) the apparent viscosity of a shear-thinning fluid is a maximum at the centre of the pipe and this aids particle suspension (though some of this effect may be offset by the propensity of migration across streamlines and the enhanced settling velocities in sheared fluids); (ii) the apparent viscosity is a minimum at the pipe wall, thus, the frictional pressure drop will be low and will increase only relatively slowly with increasing mixture velocity, hence leading to a lower power consumption; and (iii) if the fluid exhibits a yield stress, it tends to assist the suspension of coarse particles in the central region of the pipe (Chhabra and Richardson, 1999).

The use (optional or otherwise) of non-Newtonian carrier fluids for processes which involve conveying of mixtures through pipes has been restricted by a lack of understanding of the behaviour of these flows, and has only been reported in a few studies. Charles and Charles (1971) transported 216 μm sand particles in shear-thinning clay suspensions. The head loss was six times smaller compared to using water. Similarly, Ghosh and Shook (1990) reported a reduction in pressure gradient for the flow of 600 μm sand particles in a shear-thinning CMC solution, but not for 2.7 mm pea gravel particles; this was attributed to the fact that these larger particles were conveyed in the form of a sliding bed and not as a suspension. Duckworth et al. (1983, 1986) conveyed coal particles (up to 19 mm) in a slurry of fine coal which behaved as a Bingham plastic. None of these studies, however, attempted to develop a general method for the prediction of pressure gradient. Chhabra and Richardson (1985) presented a correlation for the prediction of the hydraulic pressure gradient based on experimental data relating to mixtures with a sliding bed. They concluded from a review of the literature that there were insufficient reliable results for expressions to be given for the pressure gradients in other flow regimes. More recently, Gradeck et al. (2005) reported a friction factor chart which groups data acquired using coarse alginate particles (d = 4.4 mm) flowing in Newtonian and non-Newtonian carrier fluids, at solid concentrations up to 15% v/v. The data were fitted by a simple friction factor — Reynolds number correlation.

Experimental studies of laminar solid–liquid flows are scarce and detailed measurements of the flow field and pressure drop in these systems are lacking. Some limited studies used Magnetic Resonance Imaging (McCarthy et al., 1996) or Ultrasound Doppler Velocimetry (Guer et al., 2003). Fairhurst et al. (2001) and Barigou et al. (2003) used Positron Emission Particle Tracking (PEPT) to study coarse (d = 5–10 mm) nearly neutrally-buoyant particles in non-Newtonian CMC fluids and reported information on the solid phase velocity profile and flow regimes within such suspensions. Computational modelling work in this specific area has also been limited. In a rare attempt, Krampa-Morlu et al. (2004) used CFD to predict the flow features of coarse aqueous solid–liquid slurries in turbulent upward flow including velocity profiles. The CFD model, formulated using the software CFX 4.4 (ANSYS Inc.), was tested using the experimental results of Sumner et al. (1990). The particles had a density of 2650 kg m^{-3} and a diameter of 0.47 or 1.7 mm and were simulated at concentrations up to 30% v/v. The authors concluded that the code failed to accurately predict important features of the flow using the default settings.

In this paper, a CFD model, based on the commercial code ANSYS CFX 10.0, is used to study the conveying of nearly neutrally-buoyant coarse particles in laminar non-Newtonian flow in a horizontal pipe. CFD results of the flow field and particle passage times are validated using experimental data obtained, respectively, by PEPT and Hall effect sensors from our earlier work (Barigou et al., 2003; Fairhurst et al., 2001; Fairhurst, 1998), while pressure drop predictions are compared with a number of correlations from the literature. The aim of this work is to evaluate the capability of CFD to predict such complex flows and thus facilitate their modelling for research and industrial design purposes.

2. CFD model of two-phase solid–liquid flow

2.1. Governing equations

The following equations form the basis of the CFD model used to simulate the laminar flow of coarse particles in a non-Newtonian fluid.

2.1.1. Continuity equations

Assuming isothermal flow, a continuity equation can be written for the liquid phase as follows (Van Wachem and Almstedt, 2003)

$$\frac{\partial}{\partial t}(\rho_f C_f) + \nabla \cdot (\rho_f C_f U_f) = 0 \tag{1}$$

and similarly, for the solid phase

$$\frac{\partial}{\partial t}(\rho_s C_s) + \nabla \cdot (\rho_s C_s U_s) = 0 \tag{2}$$

with the constraint

$$C_f + C_s = 1 \tag{3}$$

where the subscripts f and s denote the fluid and solid phase, respectively, C is volume fraction, ρ is density, U is the velocity vector, and t is time.

2.1.2. Momentum equations

The momentum equation for each phase is derived such that it includes, along with the forces acting on that phase, an inter-phase momentum transfer term that models the interaction between the two phases (Van Wachem and Almstedt, 2003); thus for the liquid

$$\rho_f C_f \left[\frac{\partial U_f}{\partial t} + U_f \cdot \nabla U_f\right] = -C_f \nabla P + C_f \nabla \cdot \bar{\bar{\tau}}_f + C_f \rho_f g - M \tag{4}$$

and for the solid

$$\rho_s C_s \left[\frac{\partial U_s}{\partial t} + U_s \cdot \nabla U_s\right] = -C_s \nabla P + C_s \nabla \cdot \bar{\bar{\tau}}_f + \nabla \cdot \bar{\bar{\tau}}_s - \nabla P_s + C_s \rho_s g + M \tag{5}$$

where P is pressure, g is the gravitational acceleration vector, $\bar{\bar{\tau}}$ is the viscous stress tensor, P_s is solid pressure, and M is the interfacial momentum transfer per unit volume made up of the drag force, F_d, and the lift force, F_l. The other forces on the right-hand side of the momentum equations are the pressure force, viscous force, gravitational force, as well as particle–particle interaction force for the solid phase represented by the solid pressure term. The inclusion of this term is particularly important for highly concentrated suspensions ($C_s > 0.2$) as the interactions increase with solid concentration. This solid pressure term is, therefore, a function of the solid concentration (Gidaspow, 1994), thus

$$P_s = P_s(C_s) \tag{6}$$

and therefore,

$$\nabla P_s = G(C_s) \nabla C_s \tag{7}$$

The function $G(C_s)$ is called the Elasticity Modulus, and is expressed as follows:

$$G(C_s) = G_0\, e^{E(C_s - C_{sm})} \tag{8}$$

where G_0 is the reference elasticity modulus, E is the compaction modulus, and C_{sm} is the maximum packing parameter (maximum solid loading). There are no universally accepted values for these parameters; however, the values $G_0 = 1$ Pa, $E = 20$–600, have been suggested by Bouillard et al. (1989). The maximum packing parameter C_{sm} was determined by Thomas (1965) as 0.625 for spherical particles.

2.1.3. Inter-phase drag force

The inter-phase drag force per unit volume, F_d, is expressed by (Van Wachem and Almstedt, 2003; Kleinstreuer, 2003)

$$F_d = \frac{3C_D}{4d} C_s \rho_f |U_s - U_f|(U_f - U_s) \tag{9}$$

where C_D is the drag coefficient of a single particle and d is the particle diameter. For Reynolds numbers outside Stokes flow, the drag coefficient is a function of the flow regime and is usually estimated using one of the many empirical expressions which exist (Lareo et al., 1997). For densely distributed particles of solid concentrations up to $C_s = 0.2$, the expression by Wen and Yu (1966) can be used to calculate C_D, thus

$$C_D = (1 - C_s)^{-1.65} \max\left[\frac{24}{Re'}(1 + 0.15 Re'^{0.687}), 0.44\right] \tag{10}$$

where $Re' = (1 - C_s)Re_p$, and

$$Re_p = \frac{\rho_f u_\infty d}{\mu_f} \tag{11}$$

where Re_p is the generalised particle Reynolds number which depends on the fluid effective viscosity, μ_f, and the local slip velocity between the two phases, taken here to be the sedimentation velocity, u_∞, of the particle in an infinite expanse of carrier fluid (Brown and Heywood, 1991).

For higher concentrations ($C_s > 0.2$), the Gidaspow Drag model can be used where the inter-phase drag force per unit volume is given by (Ding and Gidaspow, 1990)

$$F_d = \left[150\frac{C_s^2 \mu_f}{C_f d^2} + \frac{7 C_s \rho_f |U_s - U_f|}{4d}\right](U_f - U_s) \tag{12}$$

2.1.4. Lift force

The lift force caused by the velocity gradient is given by (Van Wachem and Almstedt, 2003)

$$F_l = C_s \rho_f C_l (U_s - U_f) \times (\nabla \times U_f) \tag{13}$$

where C_l is the lift coefficient. A wide range of values for C_l can be found in the literature (Van Wachem and Almstedt, 2003); the choice of the C_l value used in the simulations is discussed in Section 2.2.2.

2.1.5. Suspension viscosity

The presence of solid particles in a carrier fluid influences the shear rate distribution, and hence the suspension viscosity. The suspension apparent viscosity, μ_{susp}, can therefore be written in terms of the fluid apparent viscosity, μ_a, and a solid viscosity, μ_s, thus

$$\mu_{susp} = (1 - C_s)\mu_a + C_s \mu_s \tag{14}$$

Suspension viscosity is usually expressed as a relative viscosity, μ_r, defined as

$$\mu_r = \frac{\mu_{susp}}{\mu_a} \tag{15}$$

The well-known Einstein equation for estimating the relative viscosity of very dilute suspensions with negligible particle–particle interactions is given by (Einstein, 1905; Chakrabandhu and Singh, 2005)

$$\mu_r = \frac{\mu_{susp}}{\mu_a} = 1 + 2.5 C_s \tag{16}$$

For more concentrated suspensions, however, particle–particle interactions must be taken into account and modifications made to Einstein's equation resulted in expanded versions of Eq. (16). One form of the expanded Einstein equation is the following third-order expansion (Thomas, 1965)

$$\mu_r = 1 + 2.5 C_s + 10.05 C_s^2 + 20.84 C_s^3 \tag{17}$$

As noted by Thomas (1965), the third-order term in Eq. (17) accounts for particle–particle interactions. As the solids concentration increases, particle–particle interactions become more probable, thus, increasing the energy dissipation and leading to a more rapid increase of μ_r with C_s (Shook and Roco, 1991). The constants in Eq. (17) have been determined mainly for fine particles in Newtonian carrier fluids. However, they have also been used and validated for coarse particles in non-Newtonian carrier fluids by Chakrabandhu and Singh (2005). In their study, these authors evaluated various theoretical, semi-empirical, and empirical equations for the suspension relative viscosity using their experimental data obtained with non-Newtonian fluids. They concluded that Eq. (17) provided the closest estimates over the entire range of experimental variables used in their study.

2.1.6. Carrier fluid viscosity

The fluid rheology implemented in the present CFD model was that used to model the pseudoplastic CMC solutions used in our earlier experimental work (Barigou et al., 2003; Fairhurst et al., 2001). These fluids were described by the Ellis model

$$\mu_a = \frac{\mu_0}{1 + \left(\frac{\tau}{\tau_{1/2}}\right)^{\alpha - 1}} \tag{18}$$

where μ_0 is the zero-shear viscosity, τ is the shear stress, $\tau_{1/2}$ is the shear stress at which the apparent viscosity has dropped to $\mu_0/2$, and α is a measure of the degree of shear thinning. The values of the Ellis parameters employed in the simulations are those corresponding to the experimental fluids used, as shown in Table 1.

The volumetric flowrate, Q, of an Ellis fluid can be calculated from the following exact equation (Matsuhisa and Bird, 1965):

$$Q = \frac{\pi R^3 \tau_w}{4\mu_0}\left[1 + \left(\frac{4}{\alpha + 3}\right)\left(\frac{\tau_w}{\tau_{1/2}}\right)^{\alpha - 1}\right] \tag{19}$$

where R is the pipe radius, and τ_w is the wall shear stress. The fluid velocity profile can also be derived, thus (Matsuhisa and Bird, 1965)

$$u(r) = \frac{\tau_w}{\mu_0}\left[\frac{R}{2}\left(1 - \frac{r^2}{R^2}\right) + \left(\frac{\tau_w}{\tau_{1/2}}\right)^{\alpha - 1}\left(\frac{R}{\alpha + 1}\right)\left(1 - \left(\frac{r}{R}\right)^{\alpha + 1}\right)\right] \tag{20}$$

where r is radial position.

2.2. CFD simulations

The ANSYS Workbench 10.0 software package was used to set up simulations in three dimensions because of the axial asymmetry of the flow. The simulations were solved using the CFX-Solver component of the package. In the Eulerian–Eulerian multiphase model adopted here, the liquid and solid phases are regarded as

Table 1
Range of PEPT experiments and corresponding CFD simulations

CMC (% w/w)	μ_0 (Pa s)	$\tau_{1/2}$ (Pa)	α	d (mm)	ρ_s (kg m^{-3})	ρ_f (kg m^{-3})	C_s	$\bar{u}$ (mm s^{-1})	$Re_p = \frac{\rho_f u_\infty d}{\mu_f}$	$Re_t = \frac{\rho_f \bar{u} D}{\mu_f}$
0.5	0.12	6.6	2.03	5	1020	1000	0.30	65	0.075	27.2
0.5	0.12	6.6	2.03	10	1020	1000	0.30	65	0.075	27.2
0.8	0.62	7.4	2.03	10	1020	1000	0.21	34	0.012	3.0
0.8	0.62	7.4	2.03	10	1020	1000	0.21	77	0.012	8.2
0.8	0.62	7.4	2.03	10	1020	1000	0.40	24	0.012	2.1

continuous phases. It is possible to consider the solid phase as an Eulerian phase subject to an appropriate modelling of the different forces and interactions taking place. Once the interaction terms are determined, the Eulerian approach has been reported to be efficient at simulating multiphase flows (see for example, Hu et al., 2001). The Eulerian–Lagrangian model, on the other hand, is in principle more realistic in that it simulates the solid phase as a discrete phase and so allows particle tracking. However, after an evaluation of the relevant literature as well as a number of simulation trials, it was concluded that the number of dispersed particles that can be tracked within all available commercial CFD software is currently very limited, thus limiting the applicability of the Eulerian–Lagrangian model to dilute mixtures well below ~5% v/v (Van Wachem and Almstedt, 2003).

The geometry consisted of a horizontal pipe of diameter D = 45 mm, as used in the two-phase flow experiments described below. The pipe length, L, selected for flow simulation needs to be greater than the maximum entrance length, L_e, i.e. the length required for flow to fully develop. In single-phase Newtonian laminar flow, the entrance length can be estimated from (Shook and Roco, 1991)

$$\frac{L_e}{D} = 0.062 Re_t \tag{21}$$

where $Re_t = \frac{\rho_f \bar{u} D}{\mu_f}$ is the tube Reynolds number where $\bar{u}$ is the mean mixture velocity.

For two-phase solid–liquid flow a similar correlation for predicting L_e does not exist. However, given the fact that the particles considered here were nearly-neutrally buoyant, the above correlation for single phase flow would be expected to give a reasonable estimate of L_e. Moreover, the use of shear thinning fluids as well as the presence of solid particles leads to flatter velocity profiles and, hence, the estimates yielded by the above correlation are even likely to be conservative. In addition to using this criterion, a number of numerical experiments were conducted with different pipe lengths. At lower Re_t values (<200), a pipe length of 600 mm was sufficient to give fully developed flow of the suspensions considered whilst keeping computational cost low. Using a longer pipe did not affect the two-phase pressure gradient or the velocity profile of either phase. At higher Re_t values, a length of 2000 mm was used.

The geometry was meshed into tetrahedral cells, approximately 180×10^3 or 500×10^3 depending on the pipe length used. The 3D grid was optimised by conducting a mesh-independence study using different mesh sizes, starting from a coarse mesh and refining it until results were no more dependent on mesh size. Inflation layers covering about 20% of the pipe radius were created near the pipe wall in order to accurately account for the high parameter gradients in that region.

2.2.1. Single-phase fluid flow simulation

Simulations of the non-Newtonian carrier fluid flowing alone were conducted as an initial validation of the code and the numerical grid. The results were also subsequently used to reveal the effects of solid particles on the liquid velocity profile, by comparing the velocity profile of the liquid flowing alone to that which exists in a solid–liquid suspension. Furthermore, such simulations were useful in evaluating the capability of the code to predict the flow of fine particle suspensions that can be treated as homogeneous or pseudo-homogeneous and, hence, which can be represented by a non-Newtonian single phase fluid, as discussed above.

The fluid rheology was that used to model the corresponding experimental CMC solutions, i.e. using the apparent viscosity of an Ellis fluid (Eq. (18)), and the Ellis parameter values shown in Table 1. A mass flowrate boundary condition was used at the pipe inlet, while static pressure was specified at the outlet. The usual no-slip boundary condition was assumed at the pipe wall.

The advection terms in the governing momentum equation (Eq. (4) with C_f = 1 and M = 0 for single phase flow), were discretized using a second-order accurate differencing scheme, which is more accurate than a first-order scheme (Shaw, 1992). In the finite volume method used for discretizing the momentum equation, the variable value at an integration point, ϕ_{ip}, is calculated from its value at the upwind node, ϕ_{up}, and the variable gradient, $\nabla\phi$, thus

$$\phi_{ip} = \phi_{up} + \beta \nabla\phi . \Delta\vec{r} \tag{22}$$

where β is a blend factor and $\Delta\vec{r}$ is the vector from the upwind node to the integration point. The numerical scheme adopted here was the Numerical Advection Correction Scheme, wherein a constant value of β is specified and the variable gradient is calculated as the average of the adjacent nodal gradients. With β = 0, the scheme is first-order accurate; in the current simulation, β was set equal to 1 which is second-order accurate. The solution was assumed to have converged when the mass and momentum residuals reached 10^{-5} for all of the equations. This typically required ~100 iterations.

2.2.2. Two-phase solid–liquid flow simulation

The particles were introduced in the continuous liquid phase as an Eulerian solid phase. The viscosity of the solid phase was modelled using Eq. (14) with the relative suspension viscosity as given by Eq. (17). Details of the numerical simulations conducted are summarised in Table 1.

The mixture mass flowrate was specified as the boundary condition at the pipe inlet, while at the outlet static pressure was specified. The homogeneous volumetric fraction of each phase was specified at the inlet. Using flowrate as a boundary condition is the common way of formulating pipe flow problems, i.e. one designs a system to deliver a given flowrate. Note, however, that using a pressure-specified inlet boundary condition is a stricter way of testing the CFD code as a flowrate boundary condition might be perceived as a way of helping to steer the simulation towards the right solution. This option was tested but it did not affect the results of the CFD computations. At the pipe wall, two different conditions were used for the liquid and solid phases. For the liquid phase the usual no-slip condition was used, while for the solid phase free-slip was assumed in order to prevent the solid phase from adhering to the wall, which is consistent with the real flow behaviour of coarse particles near a solid boundary and is normal practice in the modelling of two-phase flows.

Due to the complexity of the solid–liquid flows considered here, simulations required a great deal of experimentation and optimisation. Of primary importance was the appropriate modelling of

forces and interactions between the two phases. The buoyancy force was taken into account by the density difference between the liquid and solid. Forces due to particle collision required the introduction of an additional "Solid Pressure" term into the solid phase momentum equation (Eq. (5)). A solid pressure model based on the Gidaspow model (Eqs. (6)–(8)) was used with default values of the model parameters: $G_0 = 1$ Pa, $E = 600$, and $C_{sm} = 0.625$. The drag force was modelled using the Wen Yu drag model (Eq. (10)) for solid concentrations up to 20% v/v, and the Gidaspow drag model (Equation (12)) for higher concentrations. It should be noted here that the particle Reynolds number (Eq. (11)) was computed based on the local apparent viscosity of the fluid used, thus taking account of the non-Newtonian behaviour of the fluid (He et al., 2001). The lift force was modelled using Eq. (13) with the default value $C_l = 0.5$; a range of C_l values were tested but they did not affect the results.

The so-called "High Resolution Scheme" was implemented in discretizing the advection terms in the governing equations. In this scheme, the value of the blend factor, β, in Eq. (22), is not constant but is calculated locally to be as close to 1 as possible without resulting in non-physical parameter values. This scheme is therefore intended to satisfy the requirements of both accuracy and boundedness. Imposing a second-order accurate scheme (i.e. $\beta = 1$) in such complex simulations may result in difficult convergence.

Numerical convergence under steady state mode could not be attained for solid–liquid flows; consequently, simulations were run in the transient mode. In steady state simulations, and due to the absence of time-dependence, the fluid acceleration is not modelled in the same way as it physically occurs. It is usually recommended that simulations of steady state nature should be run transiently when convergence difficulty is encountered, in order to enhance the stability of convergence. The modelling of time variation smooths out the way in which the solution changes from one iteration to the next (Shaw, 1992). A small time step of 0.01 s was used to help the solution converge. Eventually, the solution reached a steady state and met the convergence criterion which was set at a residual target RMS = 10^{-4}. On average, 200 time steps were required, with 1–5 iterations to achieve convergence for all of the equations at each time step.

3. Validation process of CFD simulations

As pointed out above, detailed measurements of the flow field in solid–liquid suspensions are very scarce due to the lack of suitable measurement techniques. In our earlier work (Barigou et al., 2003; Fairhurst et al., 2001; Fairhurst, 1998), we carried out extensive experiments using the technique of PEPT to determine the trajectories and velocity profile of coarse solid particles flowing in non-Newtonian CMC carrier fluids. Hall effect sensors were also used to independently measure particle passage times and, thus, provide a further set of different results for validating the CFD computations. These unique sets of experimental results are used here for the purpose of evaluating the accuracy of the numerical CFD simulations. CFD predictions of pressure drop in solid–liquid flow, on the other hand, are assessed using correlations gleaned from the literature. The validation of velocity profiles and pressure drop in single-phase fluid flow simulations was based on exact analytical equations.

3.1. PEPT validation of solid phase velocity profile

PEPT uses a single positron-emitting particle as a flow tracer which is tracked in 3D space and time within operating equipment to reveal its full Lagrangian trajectory. PEPT is unique in flow visualisation terms, being able to examine flow phenomena in three dimensions that could not be observed as effectively by using other techniques. It is particularly useful for the study of multiphase flows, to map the flow of fluids and the flow of particles, where one component can be labelled and its behaviour observed. The method allows probing of opaque fluids and within opaque apparatus, a distinct advantage over optical visualisation methods such as LDV or PIV. More details of the technique and its applications can be found in Barigou (2004), Barigou et al. (2003), and Fairhurst et al. (2001).

A gravity driven flow loop was used where the solid–liquid mixture flowed through a down pipe followed by a horizontal pipe, each of 1400 mm length and 45 mm inner diameter. The solid particles used in the experiments were alginate spheres of 5 mm and 10 mm diameters. Experiments were performed at outlet solid volumetric concentrations of 21 ± 2%, 30 ± 2% and 40 ± 2% v/v and mixture velocities ranging from 24 to 125 mm s^{-1}.

A 600 μm resin bead, containing the positron emitting radionuclide ^{18}F, was imbedded inside an alginate particle and used as a radioactive tracer. The resin bead had no measurable effect on the density of the particle. The tracer thus had the same physical properties (density, mechanical, surface roughness) as any other particle and thus flowed in the same manner through the system making the particle track obtained representative of the others. During an experimental run, single tracers were injected into the loop and collected at the exit; at least 50 particle trajectories were measured in order to obtain a representative sample (Barigou et al., 2003; Fairhurst et al., 2001).

The solid phase velocity profile was obtained using an algorithm based on calculating the velocity of particles at different radial positions. This was achieved by following a particle at a particular radial position and measuring the distance between successive locations and the time required to travel this distance. Details of the algorithm can be found in our original work (Barigou et al., 2003; Fairhurst et al., 2001).

3.2. Validation of pressure drop

Pressure drop in solid–liquid flow remains one of the most difficult parameters to predict. One of the complications in the estimation of pressure drop in such systems is the existence of different flow regimes which are dictated by the complex interaction of the many different variables involved. It is known that the presence of solid particles results in an increase in the pressure drop incurred, but there are no theoretical models available for calculating such a pressure drop. However, many empirical or semi-empirical approaches do exist, and a number of correlations from the literature were used here to verify the CFD predictions. Such correlations tend to be specific to the experimental conditions for which they were developed. Any attempt to use such correlations for other conditions is likely to lead to significant errors (Crowe et al., 1998), and therefore the correlations used here had to be selected to overlap as much as possible with the solid–liquid flows of this study.

Durand's classical empirical correlation which stands as a reference in the field (Durand, 1952), was developed using data for highly turbulent sand and gravel slurries with particle diameters in the range 0.2–25 mm, solid concentrations up to 60% v/v, and pipe diameters 38–580 mm, thus

$$\frac{i - i_w}{i_w C_s} = K\left[\frac{\bar{u}^2 C_D^{0.5}}{gd(s-1)}\right]^m \tag{23}$$

which can be written as

$$\phi = K\Psi^m \tag{24}$$

where K and m are empirical constants, and

$$\Psi = \frac{\bar{u}^2 C_D^{0.5}}{gd(s-1)} \tag{25}$$

where $\phi = \frac{i-i_w}{i_w C_s}$ is the dimensionless excess head loss, i and i_w are head losses for the solid–liquid mixture and for water flowing alone, respectively, and s is the particle–liquid density ratio. The drag coefficient, C_D, is given for a particle settling at its terminal velocity, u_∞, in an unbounded liquid by (Brown and Heywood, 1991)

$$C_D = \frac{4}{3}\frac{gd(s-1)}{u_\infty^2} \tag{26}$$

According to Dhodapkar et al. (2005), Durand's correlation should only be used for $\Psi/C_s > 40$, corresponding to fully suspended heterogeneous flow.

While m has generally been taken to be -1.5, different values of K have been used depending on the solid–liquid system considered (Zandi and Govatos, 1967; Turian et al., 1971; Turian and Yuan, 1977; Darby, 1986; Shook and Roco, 1991; Dhodapkar et al., 2005). According to Darby (1986), many of the published K values are due to a misinterpretation of Durand's work and the correct value should be 150, a value also reported by Turian et al. (1971) which accounts for the effect of particle density. Most notably, Zandi and Govatos (1967) proposed the following values which have been generally hailed as an improvement on Durand's original correlation: $K = 280$ and $m = -1.93$ for $\Psi < 10$, and $K = 6.3$ and $m = -0.354$ for $\Psi > 10$, all valid for $\Psi/C_s > 40$.

A number of authors reported that Durand's correlation which is perhaps the most widely used, has limited applicability, however. For example, Rasteiro et al. (1993) commented that Durand's correlation may deviate by over 40% from measured values. Turian et al. (1971) also reported deviations exceeding 50%. Darby (1986), on the other hand, indicated that Durand's correlation does not account for inter-particle interactions, and Babcock (1971) argued that the dimensionless groups in Durand's correlation are not sufficient to account for the influences of solids concentration, particle diameter, and pipe diameter.

In another development, Newitt et al. (1955) proposed a set of regime-specific correlations and used transition velocities to delineate the flow regimes. The transition criteria used imply that the transition from one regime to the next is abrupt, which is not the case in reality (Turian and Yuan, 1977; Shook and Roco, 1991). For the heterogeneous flow regime which is relevant to the flows considered here, the correlation was

$$\phi = 1100\frac{gDu_\infty(s-1)}{\bar{u}^3} \tag{27}$$

Rasteiro et al. (1993) considered in their semi-theoretical approach the total pressure drop in a solid–liquid system to be made up of the kinetic energy loss, E_c, the viscous energy loss, E_v, and the energy loss due to particle–particle interactions, E_p, thus

$$\left[\frac{\Delta P}{L}\right]_{susp} = A_1 E_c + A_2 E_v + A_3 E_p \tag{28}$$

where

$$E_c = \frac{\rho_f \bar{u}^2}{d(1-C_s)}; \quad E_v = \frac{\mu_f \bar{u}}{(d(1-C_s))^2}; \quad E_p = \frac{(\rho_s - \rho_f)gC_s^2}{(1-C_s)^3} \tag{29}$$

A_1, A_2, and A_3 are empirical constants which were determined by applying the method to experimental data obtained from the literature. Rasteiro et al. (1993) gave the values of these constants based on solid particles of high density (up to 2650 kg m^{-3}) and particle diameter in the range 0.16–1.28 mm in highly turbulent flow with velocities in the range 0.98–3.76 m s^{-1}. Particle concentration varied from 2% to 34% v/v. The particles under these conditions were fully suspended which qualitatively resembled the flow of the nearly-neutrally buoyant particles simulated in this work. The model was found to give improved pressure drop predictions compared to Durand's correlation.

Suspensions of fine and/or neutrally-buoyant particles can be approximated as a single phase fluid with properties equivalent to the mean properties of the suspension. This approximation allows the calculation of pressure drop as a function of the suspension Reynolds number in the same way as in single-phase flows. This approach was used by Gradeck et al. (2005) to calculate the pressure drop of fairly dilute solid–liquid suspensions with nearly-neutrally buoyant coarse alginate particles ($d = 4.4$ mm) in water and glucose solutions (Newtonian), and CMC solutions (non-Newtonian) in a 30 mm diameter pipe. The pressure drop per unit length, $\Delta P/L$, was expressed in terms of the friction factor

$$f = \frac{1}{2}\frac{\mathrm{d}}{\rho_{susp}\bar{u}^2}\frac{\Delta P}{L} \tag{30}$$

They found that for laminar flow

$$f = \frac{16}{Re_s} \tag{31}$$

where the suspension Reynolds number, Re_s, is based on the mean suspension density, ρ_{susp}, and the effective viscosity of the suspension, μ_{susp}, measured experimentally using the pressure drop–flowrate relationship for a homogeneous fluid for solid concentrations up to 15% v/v, i.e.

$$Re_s = \frac{\rho_{susp}\bar{u}D}{\mu_{susp}} \tag{32}$$

4. Results and discussion

4.1. Single-phase fluid flow

Two Ellis liquids were used as shown in Table 1. The flow field of each liquid flowing alone was obtained numerically. The predicted flowrate was within 1% of the exact solution (Eq. (19)) for the 0.5% CMC solution, and better than 3% for the more viscous 0.8% CMC solution. The numerically obtained velocity profiles are compared in Fig. 1 to the exact analytical profiles for an Ellis fluid (Eq. (20)). The agreement between theory and CFD is excellent for both fluids.

For the sake of completeness, simulations were also run for other pseudoplastic fluids of the power law type, as well as viscoplastic (i.e. yield stress) fluids of the Herschel–Bulkley and Bing-

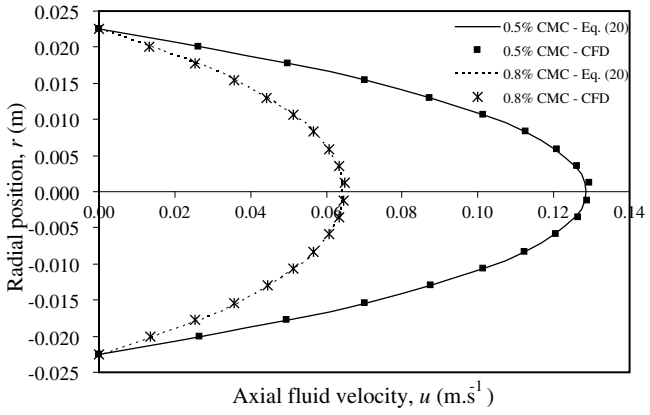

Fig. 1. Comparison of theoretical and CFD velocity profiles of Ellis fluid flowing alone: 0.5% CMC, $\bar{u} = 66$ mm s^{-1}; 0.8% CMC, $\bar{u} = 33$ mm s^{-1}.

ham plastic types which are representative of many industrial homogeneous suspensions. The velocity profiles predicted by CFD matched the theoretical ones to within a very good degree of accuracy, usually better than 3%.

4.2. Two-phase solid–liquid flow

4.2.1. Solid phase velocity profile

The CFD-predicted solid phase velocity profiles were validated using the PEPT results obtained in our earlier work (Fairhurst et al., 2001; Fairhurst, 1998), as discussed above. The cases studied are summarised in Table 1. The experimental velocity profile was obtained by dividing the pipe cross-section into eight regions: four above and four below the pipe centreline as shown in Fig. 2, thus, taking into account the observed asymmetric nature of the particulate flow. In each region, the mean and standard deviation of the particle velocity was calculated. The mean velocity in each region was then normalised by the mean mixture velocity, $\bar{u}$, across the pipe.

The CFD-predicted velocity profiles obtained for the cases considered, at a section 100 mm upstream of the pipe exit, are compared to the PEPT profiles in Figs. 3–7. There is a close agreement between CFD and experiment with the simulated profiles generally falling well within the experimental error bars. CFD simulation yields a smooth particle velocity profile because the Eulerian–Eulerian numerical model used treats the solid phase as a continuum rather than individual particles. However, such a model has proved capable of providing a good prediction of the solid phase velocity profile under a wide range of flow conditions including considerably viscous liquids and high solid concentrations up to 40% v/v.

A close examination of these velocity profiles shows that the position of the maximum particle velocity is not at the pipe centreline but slightly above it. The profiles also show that particles near the top of the pipe cross-section move significantly faster than particles at the bottom. This is a result of gravitational settling, even though the solid density is only slightly higher than that of the carrier liquid. The degree of asymmetry is affected by the solids concentration and the particle Reynolds number (Fairhurst et al., 2001; Fairhurst, 1998). The velocity profile for the lowest solids concentration (C_s = 0.21; Figs. 5 and 6) is strongly asymmetric with the point of maximum axial velocity shifted about 2.5 mm above the centreline. At C_s = 0.40 (Fig. 7), however, the radial velocity profile is much more symmetrical indicating that gravitational effects are slight; in this case, particle–particle interactions are clearly more significant. It is also noteworthy that, except near the bottom

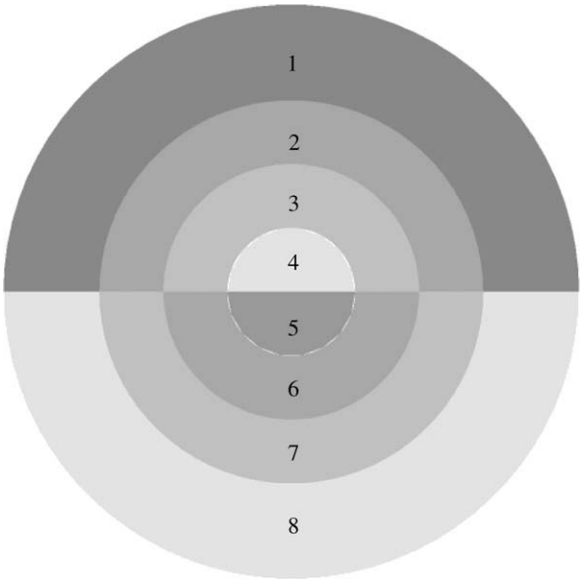

Fig. 2. Division of pipe cross-section into eight regions for solid phase velocity profile calculation.

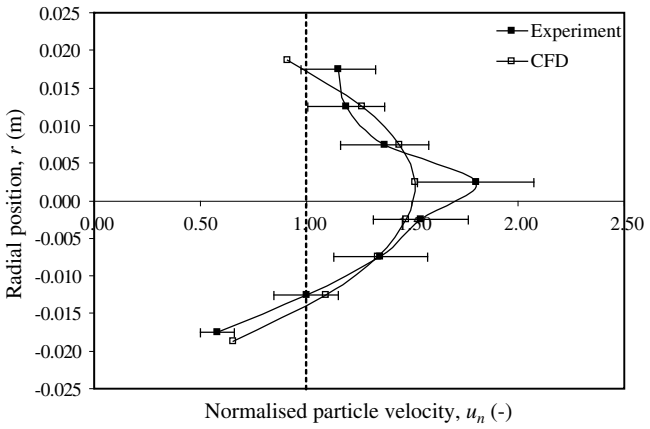

Fig. 3. CFD-predicted and experimental solid phase velocity profiles compared: 0.5% CMC; ρ_s = 1020 kg m^{-3}; d = 5 mm; C_s = 0.30; $\bar{u}$ = 65 mm s^{-1}.

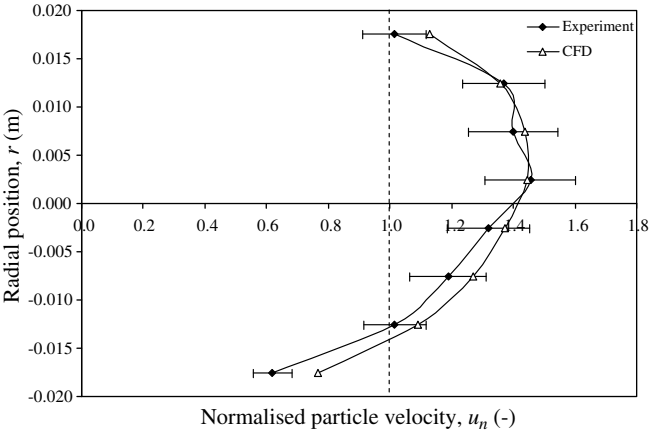

Fig. 4. CFD-predicted and experimental solid phase velocity profiles compared: 0.5% CMC; ρ_s = 1020 kg m^{-3}; d = 10 mm; C_s = 0.30; $\bar{u}$ = 65 mm s^{-1}.

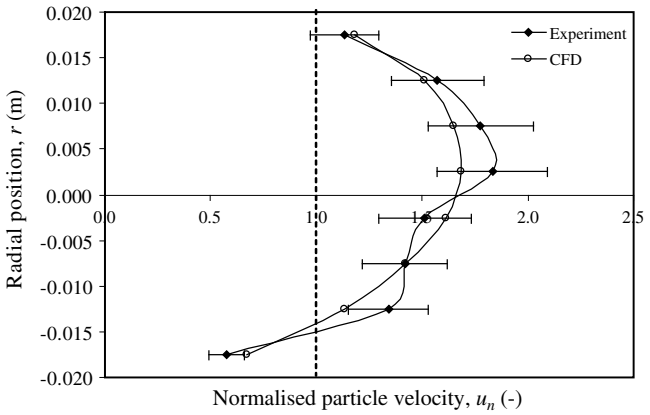

Fig. 5. CFD-predicted and experimental solid phase velocity profiles compared: 0.8% CMC; ρ_s = 1020 kg m^{-3}; d = 10 mm; C_s = 0.21; $\bar{u}$ = 34 mm s^{-1}.

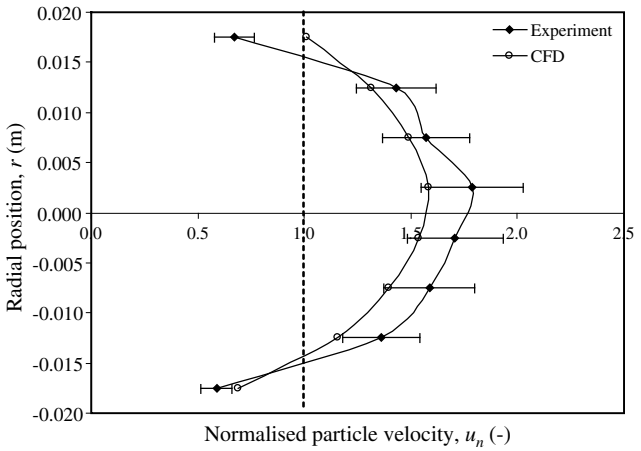

Fig. 6. CFD-predicted and experimental solid phase velocity profiles compared: 0.8% CMC; ρ_s = 1020 kg m^{-3}; d = 10 mm; C_s = 0.21; $\bar{u}$ = 77 mm s^{-1}.

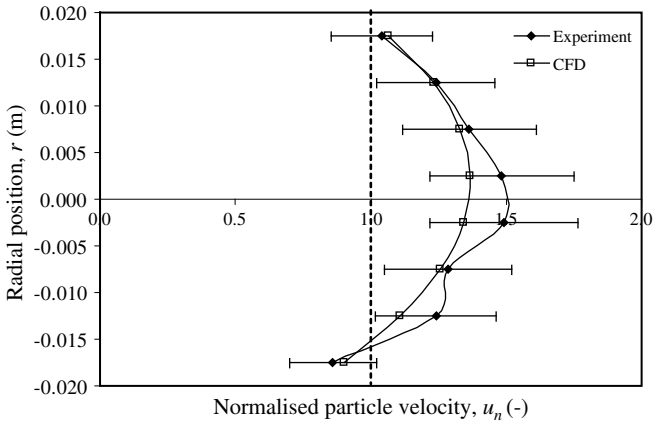

Fig. 7. CFD-predicted and experimental solid phase velocity profiles compared: 0.8% CMC; ρ_s = 1020 kg m^{-3}; d = 10 mm; C_s = 0.40; $\bar{u}$ = 24 mm s^{-1}.

of the pipe, particles generally travel faster than the mean mixture velocity, as shown in Figs. 3–7.

Another interesting feature is the velocity profile of the liquid phase and the influence of the dispersed solid phase on it. The velocity profile of the liquid in the mixture obtained by CFD is compared in Figs. 8–10 with the velocity profile of the fluid flowing alone at the same total flowrate. Results are shown for three different mixtures and flow conditions. The presence of solid particles results in a fair degree of asymmetry and flattening in the carrier fluid velocity profile. Such a flattening of the liquid velocity profile increases with solid concentration due to increased interactions between the carrier fluid and the solid particles (Figs. 9 and 10).

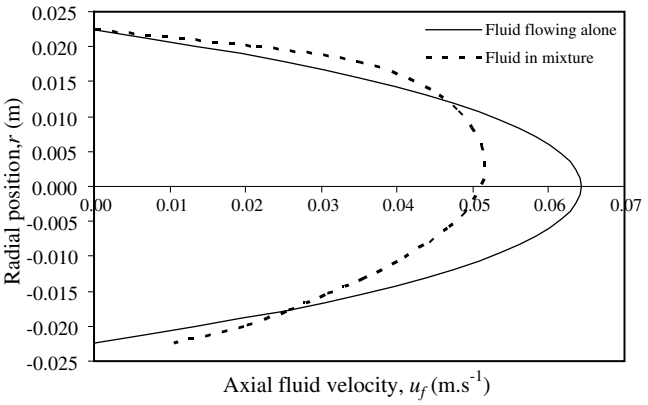

Fig. 9. Effect of solid particles on the fluid velocity profile as predicted by CFD: 0.8% CMC; ρ_s = 1020 kg m^{-3}; d = 10 mm; C_s = 0.21; $\bar{u}$ = 34 mm s^{-1}.

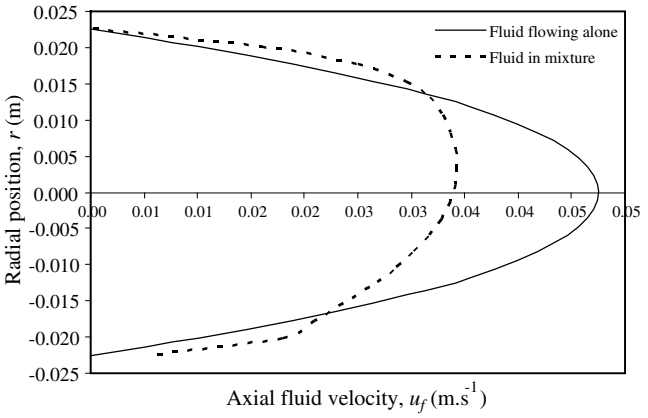

Fig. 10. Effect of solid particles on the fluid velocity profile as predicted by CFD: 0.8% CMC; ρ_s = 1020 kg m^{-3}; d = 10 mm; C_s = 0.40; $\bar{u}$ = 24 mm s^{-1}.

Fig. 11 shows the radial concentration profile of the solid phase as predicted by CFD. The results are in qualitative agreement with our earlier experimental observations, both visually and by means of PEPT particle tracks (Barigou et al., 2003; Fairhurst et al., 2001).

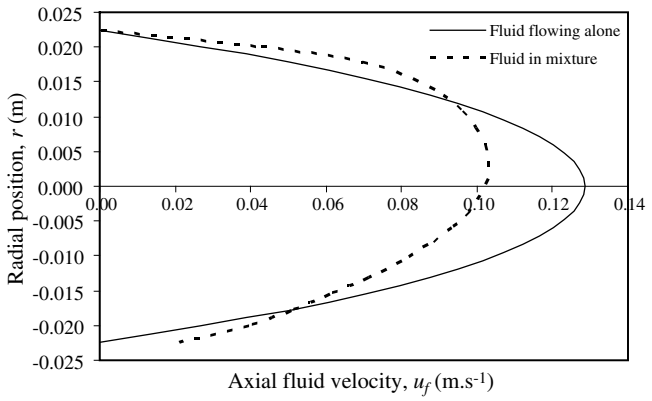

Fig. 8. Effect of solid particles on the fluid velocity profile as predicted by CFD: 0.5% CMC; ρ_s = 1020 kg m^{-3}; d = 5 mm; C_s = 0.30; $\bar{u}$ = 65 mm s^{-1}.

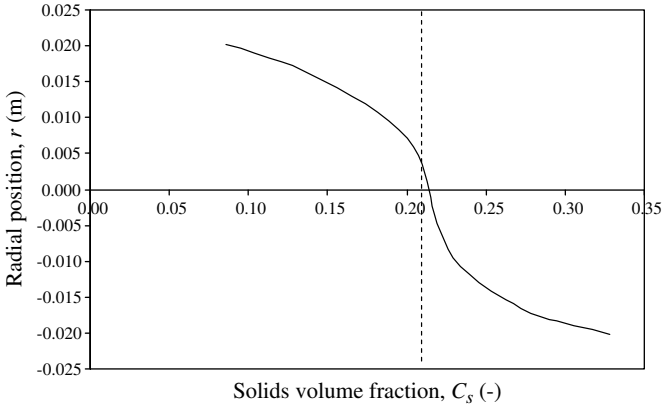

Fig. 11. Particle radial concentration profile predicted by CFD: 0.8% CMC; ρ_s = 1020 kg m^{-3}; d = 10 mm; C_s = 0.21; $\bar{u}$ = 34 mm s^{-1}.

The concentration of solid particles is relatively low in the top part of the pipe, while much higher concentrations exist near the bottom. The solid particles being slightly heavier than the fluid tend to settle out. Near the pipe centre, a region of nearly uniform concentration is observed. Such a region becomes more prominent at higher solid concentrations.

These results all have significant implications for the flow of industrial solid–liquid mixtures, such as in the thermal sterilisation of food suspensions where both the solid and liquid velocity profiles are of paramount importance in estimating the hold-tube length to deliver safe but also good quality products. However, measurement of the velocity profile is difficult in thermal food processes due to the invasive nature of most measurement techniques, opacity of the flows, the sometimes extreme processing conditions, and the inaccessibility of equipment. CFD now offers another route for gaining further understanding of solid–liquid flow systems, particularly in such complex situations.

4.2.2. Particle passage time

Prediction of particle passage times is sometimes required, for example in particulate food processing, as discussed above. It is important to be able to predict both the minimum and maximum passage times of particles in the heating and holding sections of the system, and ideally the whole distribution of passage times should be known. In our earlier work (Barigou et al., 2003; Fairhurst et al., 2001), the particle passage time was determined experimentally using Hall effect sensors (Tucker and Heydon, 1998). At least 50 passage times were measured in each experiment. By tracing a large number of representative particles, the minimum, maximum, and mean passage times were determined and then normalised by the average mixture passage time. The normalised minimum, nPT_{min}, maximum, nPT_{max}, and mean passage time, nPT_{mean} were computed from the numerically simulated solid phase velocity profile.

The CFD predictions of passage time matched to a very good degree of accuracy the experimentally determined passage time values, with a maximum deviation of 10%, as shown in Table 2. This provided a further independent validation of the CFD results. Results showed that increasing the particle diameter at the same concentration increased nPT_{min}, which corresponds to the fastest flowing particles in the flow, while reducing nPT_{max}, which in turn corresponds to the slowest moving particles. Increasing the particle concentration had a similar effect.

4.2.3. Solid–liquid pressure drop

CFD simulations were performed using a range of particle diameters, solid concentrations and Reynolds numbers, as shown in Table 3. The pressure drop was computed over a short length of pipe in the downstream half of the flow. No experimental data could be found in the literature for the type of suspension considered here, i.e. coarse particles in non-Newtonian or even Newtonian laminar flow. Therefore, the CFD predictions were compared with those yielded by Gradeck et al.'s correlation (Eq. (31)); the correlation of Durand (Eq. (24)) in its original form ($K = 150$; $m = -1.5$), and in its modified form as proposed by Zandi and Govatos; the correlation advanced by Newitt et al. (Eq. (27)); and the correlation proposed by Rasteiro et al. (Eq. (28)). These correlations were considered particularly pertinent because of their apparent suitability to flows with a high particle concentration, and the fact that the experiments upon which they were based related to flow regimes of suspended particles similar to the ones studied here.

Overall, Rasteiro et al.'s semi-empirical correlation provided the best agreement with CFD, as shown in Table 3. In most of the cases studied, the agreement was within ~15% even at high solids concentrations, which can be considered very good considering the complexity of the flow. Agreement between CFD and Gradeck et al.'s correlation was also very good (~10%) at low solids concentrations, but deteriorated at higher concentrations which were out-

Table 2
Particle passage time: CFD and experimental measurements compared

CMC (% w/w)	d (mm)	$\bar{u}$ (mm s^{-1})	C_s	$Re_t = \frac{\rho_f \bar{u} D}{\mu_f}$	nPT_{min}		nPT_{max}		nPT_{mean}	
					Experiment	CFD	Experiment	CFD	Experiment	CFD
0.5	10	230	0.31	106	0.74	0.71 (−4%)[a]	1.11	1.19 (+7%)	0.92	0.99 (+8%)
0.5	5	230	0.32	106	0.67	0.67 (0%)	1.60	1.51 (−6%)	0.98	1.00 (+2%)
0.5	5	230	0.41	106	0.84	0.76 (−10%)	1.16	1.15 (−1%)	0.93	0.99 (+7%)

[a] Deviation of CFD prediction from experimental data.

Table 3
Comparison of CFD predictions of solid–liquid pressure drop with the literature correlations

d (mm)	C_s	ρ_s (kg m^{-3})	$\bar{u}$ (m s^{-1})	$Re_t = \frac{\rho_f \bar{u} D}{\mu_f}$	$\Delta P/L$ (Pa m^{-1})					
					CFD	Rasteiro et al. (1993)	Gradeck et al. (2005)	Newitt et al. (1955)	Zandi and Govatos (1967)	Durand (1952)
						Eq. (28)	Eq. (31)	Eq. (27)	Eq. (24)[b]	Eq. (24)[c]
2	0.20	1020	0.221	100	624	629 (−1%)[a]	719 (−13%)	379 (+65%)	411 (+52%)	353 (+77%)
	0.30	1020	0.221	100	848	815 (+4%)	1116 (−24%)	394 (+115%)	442 (+92%)	354 (+140%)
	0.40	1020	0.221	100	1070	1104 (−3%)	1712 (−38%)	408 (+162%)	473 (+126%)	357 (+200%)
5	0.20	1020	0.221	100	555	629 (−12%)	719 (−23%)	524 (+6%)	448 (+24%)	369 (+50%)
	0.30	1020	0.221	100	731	815 (−10%)	1116 (−34%)	612 (+19%)	498 (+47%)	378 (+93%)
	0.40	1020	0.221	100	928	1104 (−16%)	1712 (−46%)	699 (+33%)	547 (+70%)	387 (+140%)
5	0.10	1020	0.022	10	46	49 (−6%)	48 (−4%)	NA	NA	NA
	0.10	1020	0.221	100	452	498 (−9%)	478 (−5%)	437 (+3%)	499 (−9%)	359 (+26%)
	0.10	1020	1.107	500	2448	2479 (−1%)	2394 (+2%)	1757 (+36%)	1831 (+34%)	1754 (+40%)
10	0.10	1020	0.022	10	42	49 (−15%)	48 (−12%)	NA	NA	NA
	0.20	1020	0.221	100	488	629 (−22%)	719 (−32%)	1040 (−53%)	491 (−1%)	431 (+13%)

[a] Deviation of CFD prediction from correlation.
[b] $K = 280$, $m = -1.93$ for $\Psi < 10$; $K = 6.3$, $m = -0.354$ for $\Psi > 10$.
[c] $K = 150$, $m = -1.5$.

side the range of their experimental data and therefore fell outside the correlation's range of validity (i.e. $C_s > 15\%$ v/v).

The agreement with Durand's and Zandi and Govatos' correlations was much less satisfactory, with deviations exceeding 100% in some cases. Disagreement seems to worsen as particle concentration increases, particle diameter decreases or Reynolds number increases. Rasteiro et al. (1993) also reported considerable deviations of about 40% when comparing Durand's correlation with a large set of experimental data from the literature including their own. Shook and Roco (1991) and more recently Dhodapkar et al. (2005) stated that Durand's correlation and its modified versions are not recommended for suspensions with coarse particles, but they did not justify their statement.

The results reported in Table 3 show that the prediction of pressure drop according to Durand's correlation showed little influence of solids concentration on pressure drop, in agreement with the reported observations of Babcock (1971), who found that the groups included in Durand's correlation were not sufficient to account for the influence of solids concentration and particle size. At all concentrations, the predicted pressure drop in solid–liquid flow was only slightly higher than for the fluid flowing alone, whereas CFD and other correlations (Gradeck et al., Rasteiro et al.) predicted much higher pressure drops due the presence of the solids, sometimes as much as a threefold increase at high concentrations.

Newitt et al.'s correlation was slightly more sensitive to solids concentration, but for a given concentration it showed a significant reduction in pressure drop with decreasing particle diameter contrary to an expected moderate increase because of the corresponding higher number of particles. Durand's and Zandi and Govatos' correlations seem to suffer from the same deficiency but to a lesser degree. Gradeck et al.'s and Rasteiro et al.'s correlations do not incorporate the effect of particle diameter, as shown in Table 3. All these effects, however, were predicted by CFD.

An exhaustive validation of CFD would require more extensive experimental data on pressure drop, which are presently unavailable in the literature. Nonetheless, the study conducted here has shown that, overall, CFD is capable of giving reasonable predictions of this important design parameter.

5. Conclusions

CFD simulations of solid–liquid suspension flow of coarse, nearly-neutrally buoyant particles in non-Newtonian fluids were performed using an Eulerian–Eulerian numerical model in order to assess the capability of CFD to predict the main features of such flows, namely, carrier fluid and solid phase velocity profiles, particle passage times, and mixture pressure drop. The Eulerian–Eulerian CFD model used within CFX 10.0 was capable of predicting the velocity profile of the carrier liquid flowing alone to an excellent degree of accuracy, in comparison to the exact theoretical velocity profile. Results showed that CFD is, thus, also capable of predicting the flow of homogeneous suspensions which can be approximated by single phase rheology such as pseudoplastic and viscoplastic types which are representative of many industrial suspensions.

The solid phase velocity profiles predicted by CFD matched the experimentally determined velocity profiles obtained by PEPT to a very good degree of accuracy. These velocity profiles showed that particles near the top of the pipe cross-section moved significantly faster than particles at the bottom. They also showed that the position of the maximum particle velocity was not at the pipe centreline but a few millimetres above it. The presence of solid particles resulted in a significant degree of asymmetry and flattening in the carrier fluid velocity profile, especially at high solids concentrations.

Minimum, maximum, and mean particle passage times measured by Hall effect sensors also agreed very well with CFD computations. The prediction of particle passage time has significant implications for the flow of industrial solid–liquid suspensions, as for example in the thermal sterilisation of food suspensions where sterility must be ensured without overcooking the solid particles.

CFD predictions of solid–liquid pressure drop showed a good agreement over the range of conditions studied with the semi-empirical correlation of Rasteiro et al. (1993), as well as with the more recent correlation of Gradeck et al. (2005) at low solid concentrations. Other older correlations (Durand, 1952; Zandi and Govatos, 1967; Newitt et al., 1955) showed much larger deviations from CFD, exceeding 100% in some cases. Their limitations in predicting the effects of solids concentration and particle size have been demonstrated.

Whilst a thorough validation of CFD would require more extensive experimental data on pressure drop, which are presently unavailable in the literature, the study conducted here has shown that, overall, CFD is capable of giving predictions which are no worse but probably more reliable than the correlations available in the literature as it is based on a full solution of the flow field.

References

Abulnaga, B.E., 2002. Slurry Systems Handbook. McGraw-Hill, New York.

Babcock, H.A., 1971. Heterogeneous flow of heterogeneous solids. In: Zandi, I. (Ed.), Advances in Solid–Liquid Flow in Pipes and its Application. Pergamon Press, New York, pp. 125–148.

Barigou, M., 2004. Particle tracking in opaque mixing systems: an overview of the capabilities of positron emission tomography. Chem. Eng. Res. Des. 82, 1258–1267.

Barigou, M., Fairhurst, P.G., Fryer, P.J., Pain, J.-P., 2003. Concentric flow regime of solid–liquid food suspensions: theory and experiment. Chem. Eng. Sci. 58, 1671–1686.

Bouillard, J.X., Lyczkowski, R.W., Gidaspow, D., 1989. Porosity distribution in a fluidised bed with an immersed obstacle. AIChE J. 35, 908–922.

Brown, N.P., Heywood, N.I., 1991. Slurry Handling: Design of Solid–Liquid Systems. Elsevier Science, Amsterdam.

Chakrabandhu, K., Singh, R.K., 2005. Rheological properties of coarse food suspensions in tube flow at high temperatures. J. Food Eng. 66, 117–128.

Charles, M.E., Charles, R.A., 1971. In: Zandi, I. (Ed.), Advances in Solid–Liquid Flow and its Applications. Pergamon Press, New York, p. 187.

Chhabra, R.P., Richardson, J.F., 1985. Hydraulic transport of coarse particles in viscous Newtonian and non-Newtonian media in a horizontal pipe. Chem. Eng. Res. Des. 63, 390–397.

Chhabra, R.P., Richardson, J.F., 1999. Non-Newtonian Flow in The Process Industries: Fundamentals and Engineering Applications. Butterworth–Heinemann, London.

Crowe, C.T., Sommerfeld, M., Tsuji, Y., 1998. Multiphase Flows with Droplets and Particles. CRC Press LLC, Boca Raton, FL.

Darby, R., 1986. Encyclopedia of Fluid Mechanics. In: Cheremisinoff, N.P. (Ed.), Slurry Flow Technology, vol. 5. Gulf Publishing Company, Houston, TX.

Dhodapkar, S., Jacobs, K., Hu, S., 2005. In: Crowe, C.T. (Ed.), Multiphase Flow Handbook. Fluid–Solid Transport in Ducts. CRC Press, Boca Raton, FL.

Ding, J., Gidaspow, D., 1990. A bubbling fluidization model using kinetic theory of granular flow. AIChE J. 36, 523–538.

Duckworth, R.A., Pullum, L., Lockyear, C.F., 1983. The hydraulic transport of coarse coal at high concentration. J. Pipeline 3, 251–265.

Duckworth, R.A., Pullum, L., Addie, G.R., Lockyear, C.F., 1986. Pipeline transport of coarse materials in a non-Newtonian carrier fluid. Hydrotransport 10, Paper C2, pp. 69–88.

Durand, R., 1952. The hydraulic transportation of coal and other materials in pipes, Colloq. of National Coal Board, London. Cited in Wasp, E.J., Kenny, J.P., Ghandi, R.L., 1979. Solid–liquid flow: slurry pipeline transportation. Trans Tech Publications, Clausthal, Germany.

Einstein, A., 1905. Eine neue Bestimmung der Moleküldimensionen. Ann. Physik 19, 289–306, 34, 591–597. [English translation in Einstein, A., 1956. Investigations on the theory of Brownian movements. A.D. Cooper (Trans.), R. Furth (Ed.). Dover Publications, New York].

Fairhurst, P.G., 1998. Contribution to the study of the flow behaviour of large nearly neutrally buoyant spheres in non-Newtonian media: application to HTST processing, Ph.D. Thesis, Université de Technologie de Compiègne, France.

Fairhurst, P.G., Barigou, M., Fryer, P.J., Pain, J.-P., Parker, D.J., 2001. Using positron emission particle tracking (PEPT) to study nearly neutrally buoyant particles in high solid fraction pipe flow. Int. J. Multiphase Flow 27, 1881–1901.

Ghosh, T., Shook, C.A., 1990. In: Liu, H., Round, G.F. (Eds.), Freight Pipelines. Hemisphere, Washington, DC, p. 281.

Gidaspow, D., 1994. Multiphase Flow and Fluidisation: Continuum and Kinetic Theory Descriptions. Academic Press, London.

Gradeck, M., Fagla, B.F.Z., Baravian, C., Lebouché, M., 2005. Technical note: Experimental thermomechanic study of Newtonian and non-Newtonian suspension flows. Int. J. Heat Mass Transf. 48, 3469–3477.

Guer, Y. LE., Reghem, P., Petit, I., Stutz, B., 2003. Experimental study of a buoyant particle dispersion in pipe flow. Trans. IChemE A 81, 1136–1143.

He, Y.B., Laskowski, J.S., Klein, B., 2001. Particle movement in non-Newtonian slurries: the effect of yield stress on dense medium separation. Chem. Eng. Sci. 56, 2991–2998.

Hu, H.H., Patankar, N.A., Zhu, M.Y., 2001. Direct numerical simulations of fluid–solid systems using the arbitrary Lagrangian–Eulerian technique. J. Comput. Phys. 169, 427–462.

Kleinstreuer, C., 2003. Two-Phase Flow: Theory and Applications. Taylor & Francis, London.

Krampa-Morlu, F.N., Bergstrom, D.J., Bugg, J.D., Sanders, R.S., Schaan, J., 2004. Numerical simulation of dense coarse particle slurry flows in a vertical pipe. In: 5th International Conference on Multiphase Flow, ICMF'04, paper No. 460.

Lareo, C., Fryer, P.J., Barigou, M., 1997. The fluid mechanics of two-phase solid–liquid food flows: a review. Trans. IChemE C 75, 73–105.

Matsuhisa, S., Bird, R.B., 1965. Analytical and numerical solutions for laminar flow of the non-Newtonian Ellis fluid. AIChE J. 11, 588–595.

McCarthy, K.L., Kauten, R.J., Walton, J.H., 1996. Dynamics of fluid/particulate mixtures in tube flow. Short Communication. Magn. Reson. Imaging 14, 995–997.

Newitt, D.M., Richardson, J.F., Abbott, M., Turtle, R.B., 1955. Hydraulic conveying of solids in horizontal pipes. Trans. Inst. Chem. Engrs. 33, 93–110.

Rasteiro, M.G., Figueiredo, M.M., Franco, H., 1993. Pressure drop for solid/liquid flow in pipes. Particul. Sci. Technol. 11, 147–155.

Shaw, C.T., 1992. Using Computational Fluid Dynamics. Prentice-Hall International (UK) Ltd, Englewood Cliffs, NJ.

Shook, C.A., Roco, M.C., 1991. Slurry Flow: Principles and Practice. Butterworth–Heimemann, London.

Sumner, R.J., McKibben, M.J., Shook, C.A., 1990. Concentration and velocity distributions in turbulent vertical slurry flows. Ecoulements Solide-Liquide 2, 33–42.

Thomas, D.G., 1965. Transport characteristics of suspensions. Part VIII. A note on the viscosity of Newtonian suspensions of uniform spherical particles. J. Colloid Sci. 20, 267–277.

Tucker, G.S., Heydon, C., 1998. Food particle residence time measurement for the design of commercial tubular exchangers suitable for processing suspensions of solids in liquids. Trans. IChemE C 76, 208–216.

Turian, R.M., Yuan, T.F., 1977. Flow of Slurries in Pipelines. AIChE J. 23, 232–243.

Turian, R.M., Yuan, T.F., Giacomo, M., 1971. Pressure drop correlation for pipeline flow of solid–liquid suspensions. AIChE J. 17, 809–817.

Van Wachem, B.G.M., Almstedt, A.E., 2003. Methods for multiphase computational fluid dynamics. Chem. Eng. J. 96, 81–98.

Wen, C.Y., Yu, Y.H., 1966. Mechanics of Fluidization. Chem. Eng. Prog. Symp. Ser. 62, 100–108.

Zandi, I., Govatos, G., 1967. Heterogeneous flow of solids in pipelines. In: Proceedings of the American Society of Civil Engineers. J. Hydraul. Div. 93, 145–159.